A THERMO-MECHANICAL FORMULATION FOR THE MODELING OF DISCRETE PARTICLE SYSTEMS

Conference Paper · November 2019

CITATION
1

READS
94

2 authors:

Osvaldo D. Quintana-Ruiz
University of São Paulo
8 PUBLICATIONS **5** CITATIONS
SEE PROFILE

Eduardo M. B. Campello
University of São Paulo
44 PUBLICATIONS **469** CITATIONS
SEE PROFILE

XL CILAMCE
IBERO-LATIN AMERICAN CONGRESS ON COMPUTATIONAL METHODS IN ENGINEERING
NOVEMBER 11-14, 2019
Praiamar Natal Hotel & Convention Natal, RN-BRAZIL

A THERMO-MECHANICAL FORMULATION FOR THE MODELING OF DISCRETE PARTICLE SYSTEMS

Osvaldo D. Quintana-Ruiz
Eduardo M. B. Campello
quintana.ruiz@usp.br
campello@usp.br
Dept. Structural and Geotechnical Engineering, University of São Paulo
P.O. Box 61548, 05424-970, São Paulo, SP, Brazil

Abstract. Modern industry, such as aerospace, automotive and military fields, have adopted advanced manufacturing (such as 3D printing and other particle deposition processes) as a rapid and efficient alternative for manufacturing industrial parts. Also, state-of-the-art techniques in the civil engineering industry include 3D concrete printing and cement-based additive manufacturing processes. All these techniques invariably include thermally-active particles, such as sintering powders and functionalized cementitious materials. The purpose of this work is to present a multiphysics computational model for the simulation of problems involving thermally-active particles forming discrete particle systems. Our approach is based on the Discrete Element Method (DEM), combined with lumped heat transfer equations to describe the various thermal phenomena that may take place for such systems. Particles´ motion and their thermal states over time are computed under the influence of body (e.g. gravitational) forces, contact and friction forces (and the related moments w.r.t the particles´ centers), as well as applied heat from external devices, heat transfer through conduction (upon contact with other particles and objects), convective cooling and radiative effects. The paper then develops direct, large-scale numerical simulations to illustrate the validity of the proposed scheme and its practical use to the simulation of modern engineering applications.

Keywords: Particles, thermo-mechanical effects, multiphysical particle systems, advanced manufacturing and 3D printing, discrete element method (DEM).

1 Introduction

After water, granular and particulate materials are the most processed materials in industry and engineering [1]. Modern industry, such as aerospace, automotive and military fields, have adopted advanced manufacturing (such as 3D printing and other additive particle deposition processes) as a rapid and efficient alternative for manufacturing industrial parts [2]. According to Cotteleer et al. [3], NASA used seventy 3D-printed parts for Mars Rover vehicles. Also, in the civil engineering industry state-of-the-art applications include 3D concrete printing and cement-based additive manufacturing processes. Currently, available high-performance cement-based materials cannot be directly 3D-printed, because of inadequate rheological and stiffness properties, in which temperature plays an important role. In general, additive manufacturing can provide innumerous benefits which may include: (i) enabling product design shapes that are hard (if not impossible) to create using traditional process; (ii) reduced energy consumption; and (iii) reduced material usage [2], to cite just a few. Additive manufacturing techniques invariably include thermally-active particles, such as sintering powders and functionalized cementitious materials. From a mechanistic point of view, these particles constitute discrete particle systems, which may be subjected to a range of multiphysical effects. In order to have a reliable and fairly accurate representation of their behavior under external (both thermal and mechanical) excitations, a multiphysical description is required.

With regards to heat transfer in particulate systems, it can be found in the literature that the conduction contribution is often considered the most significant for such systems, which depends on the conductivity of the solid (particles´) material, the inter-particle contacts (which are one source of coupling beteeen the thermal and mechanical fields) and the structure of the particle packing [4] [5]. But other contributions, such as convective cooling and radiative effects, may likewise play an important role. Researching on heat transfer in granular media dates back to the 1960s, focused on the modeling and understanding of both radiation and conduction phenomena across granular materials [4]. Understanding and modelling the dynamic behaviour of the mechanical and thermal states of granular materials has been a major research focus for many years since then, and discrete particle simulation plays an important role in this area. This technique became an efficient analysis tool that may provide very rich information at any desired time instant, such as the trajectories of and transient forces acting on individual particles, which is difficult (if not impossible) to obtain by conventional experimental techniques [6]. In this context, the purpose of this work is to present a multiphysics computational model for the simulation of problems involving thermally-active particles forming discrete particle systems. Our approach is based on the discrete element method (DEM) for description the particles´ dynamics, combined with simple (lumped) heat transfer equations to describe the various thermal phenomena that may take place when the system is excited by temperature gradients and external heat sources. We are able to track the motion of the particles and their thermal states over time under the influence of body (e.g. gravitational) forces, contact and friction forces (and the related moments w.r.t the particles´ centers), as well as applied heat from external devices, heat transfer through conduction (at the particles´ interfaces upon contact with other particles and objects), convective cooling and radiative effects. The model is relatively simple and straightforward to be implemented by engineers and analysts interested in the field, and may be a useful tool for practical, rapid process simulation, design and analysis. The paper then develops direct, large-scale numerical simulations to validate our scheme and illustrate its applicability to the simulation of modern engineering applications.

The DEM formulation that we adopt here is that of Campello [7], [8] and [9]. We will present it here in a summarized way, just to provide an overview of our discrete particle approach and introduce our notation. For a more detailed report, we refer the interested reader to the above-mentioned references. Our strategy to account for thermal effects into the DEM description follows the same general ideas as those of Zohdi [10] and [11]. But it has some distinguished features which make it different from Zohdi´s model: (i) we adopt a fully consistent stick-slip friction model (this is the friction type that is most frequently observed in dry granula materials [12]) for arbitrarily rotational particles; (ii) we take rolling resistance into account and (iii) we consider convective and radiative effects into the particles´ cooling behavior. Another distinction is that we use contact and heat conduction parameters that are based on physical models, in contrast to Zohdi's model, which adopts “general” parameters that

require problem-dependent calibration.

The paper is organized as follows. In section 2 we briefly describe our DEM formulation, with the various force and moment contributions that govern the particles´ dynamics and their corresponding equations of motion. In section 3 we introduce our approach to incorporate thermal effects into the system´s description, including detailed accounts of each possible heat transfer mechanism. In section 4 we present our numerical method for solution of the system´s equations, leading to a multiphysics (thermo-mechanical) solution strategy embedded within an explicit time integration scheme (we also include an algorithmic overview). In section 5 we show a few numerical examples to validate our model and illustrate its applicability, and in section 6 we close the paper with our conclusions and final considerations. Throughout the text, plain italic letters ($a, b, \ldots, \alpha, \beta, \ldots, A, B, \ldots$) denote scalar quantities, whereas boldface italic letters ($\boldsymbol{a}, \boldsymbol{b}, \ldots, \boldsymbol{\alpha}, \boldsymbol{\beta}, \ldots, \boldsymbol{A}, \boldsymbol{B}, \ldots$) denote vectors in a three-dimensional Euclidean space. The (standard) inner product of two vectors is denoted by $\boldsymbol{u} \cdot \boldsymbol{v}$, and the norm of a vector by $\|\boldsymbol{u}\| = \sqrt{\boldsymbol{u} \cdot \boldsymbol{u}}$. Notation with a superposed dot is adopted to designate time derivatives.

2 Particles' dynamics

We consider only spherical particles here. Let us assume a system of N_P particles, each with mass m_i, radius r_i and rotational inertia (relative to the particle´s center) $j_i = (2/5) m_i r_i^2$, $i = 1, \ldots, N_P$. We denote the position vector of a particle by $\boldsymbol{x}_i$, the velocity vector by $\boldsymbol{v}_i$, the incremental rotation vector by $\boldsymbol{\alpha}_i^{\Delta}$ (this is the rotation vector relative to two consecutive configurations) and the spin vector by $\boldsymbol{\omega}_i$. Following classical (Newton-Euler) dynamics, the equations of motion for the i^{th} particle are

$$\begin{aligned} m_i \dot{\boldsymbol{v}}_i &= m_i \boldsymbol{g} + \boldsymbol{f}_i^{con} + \boldsymbol{f}_i^{fric}, \\ j_i \dot{\boldsymbol{\omega}}_i &= \boldsymbol{m}_i^{fric} + \boldsymbol{m}_i^{rol}, \end{aligned} \tag{1}$$

where $\boldsymbol{g}$ is the gravity acceleration vector, $\boldsymbol{f}_i^{con}$ are the forces due to mechanical contacts (or collisions) with other particles and objects, $\boldsymbol{f}_i^{fric}$ are the forces due to friction (which arise from these contacts or collisions), $\boldsymbol{m}_i^{fric}$ is the moment due to the friction forces and $\boldsymbol{m}_i^{rol}$ is the moment induced by rolling resistance effects. The contact forces are given as a function of the amount of overlap between any two contacting particles (or a particle and an object). When a pair-wise contact is detected, we follow Hertz contact theory (see Johnson [13]) and adopt the following expression:

$$\boldsymbol{f}_i^{con} = \sum_{j=1}^{N_i^c} \boldsymbol{f}_{ij}^{con}, \quad \text{with} \quad \boldsymbol{f}_{ij}^{con} = -\frac{4}{3} \sqrt{r^*} E^* \delta_{ij}^{3/2} \boldsymbol{n}_{ij} - d^{con} \dot{\delta}_{ij} \boldsymbol{n}_{ij} \,, \tag{2}$$

where $\boldsymbol{f}_{ij}^{con}$ is the force that acts on particle i due to its contact with particle (or object) j, N_i^c is the number of particles and objects that are in contact with particle i,

$$r^* = \frac{r_i r_j}{r_i + r_j} \quad \text{and} \quad E^* = \frac{E_i E_j}{E_j (1 - \nu_i^2) + E_i (1 - \nu_j^2)} \tag{3}$$

are the effective radius and the effective elasticity modulus of the i-j contacting pair (in which E_i, E_j , ν_i and ν_j are the elasticity modulus and the Poisson coefficient of i and j, respectively), and δ_{ij} is the overlap between the pair, which is given by

$$\delta_{ij} = r_i + r_j - \|\boldsymbol{x}_i - \boldsymbol{x}_j\|. \tag{4}$$

Still in equation (2), $\boldsymbol{n}_{ij}$ is the normal contact direction, or unit vector that points from the center of particle i to the center of particle (or object) j, i.e.,

$$\boldsymbol{n}_{ij} = \frac{\boldsymbol{x}_j - \boldsymbol{x}_i}{\|\boldsymbol{x}_j - \boldsymbol{x}_i\|}, \tag{5}$$

whereas d^{con} is the contact´s damping constant (related to viscous energy dissipation in the normal direction), given by

$$d^{con} = 2\xi^{con}\sqrt{2E^* m^* \sqrt{r^*}\delta_{ij}^{1/4}}, \quad \text{with} \quad m^* = \frac{m_i m_j}{m_i + m_j}, \tag{6}$$

and $\dot{\delta}_{ij}$ is the overlap velocity of the contacting pair (i.e., relative velocity of the pair in the pair´s normal direction). In (6), ξ^{con} is the damping rate of the contact, which must be given (typically, one has $0 \leq \xi^{con} \leq 1$, with $\xi^{con} = 0$ for a perfectly elastic contact and $\xi^{con} = 1$ for a critically damped one).

The friction forces are given by Mindlin´s elastic solution for sticking contact between spheres, combined with Coulomb´s law for whenever there is sliding (i.e., dynamic friction). Accordingly, first we consider an elastic "trial stick state" in which the friction force is

$$\boldsymbol{f}_i^{fric} = \sum_{j=1}^{N_i^c} \boldsymbol{f}_{ij}^{fric,\text{trial}}, \quad \text{with} \quad \boldsymbol{f}_{ij}^{fric,\text{trial}} = -8G^*\sqrt{r^*}\delta_{ij}^{1/2}\Delta\boldsymbol{x}_{ij}^{\text{trial}} - d^{fric}\boldsymbol{v}_{ij,t}, \tag{7}$$

and then we verify it by a slip check against the static friction limit:

$$\begin{cases} IF \;\; \left\|\boldsymbol{f}_{ij}^{fric,\text{trial}}\right\| \leq \mu_s \left\|\boldsymbol{f}_{ij}^{con}\right\| \Rightarrow \boldsymbol{f}_{ij}^{fric} = \boldsymbol{f}_{ij}^{fric,\text{trial}} \;\; (\text{trial state is valid}); \\ IF \;\; \left\|\boldsymbol{f}_{ij}^{fric,\text{trial}}\right\| > \mu_d \left\|\boldsymbol{f}_{ij}^{con}\right\| \Rightarrow \boldsymbol{f}_{ij}^{fric} = \mu_d \left\|\boldsymbol{f}_{ij}^{con}\right\| \boldsymbol{t}_{ij} \;\; (\text{sliding occurs}). \end{cases} \tag{8}$$

In the above expressions, G^* is the effective shear modulus of the contacting pair (which is a function of the pair´s individual shear moduli), $\Delta\boldsymbol{x}_{ij}^{\text{trial}}$ is the pair´s trial elastic deformation in the tangential direction, d^{fric} is a friction damping constant (analogous to d^{con} in (6), as to allow for viscous energy dissipation in the tangential direction) and $\boldsymbol{v}_{ij,t}$ is the tangential relative velocity between the contact points of i and j, respectively. In (8), μ_s and μ_d are the static and dynamic friction coefficients, whereas $\boldsymbol{t}_{ij} = \boldsymbol{v}_{ij,t}\left\|\boldsymbol{v}_{ij,t}\right\|^{-1}$ is the tangential (or sliding) direction of the pair. The pair´s elastic deformation has to be computed through time integration of its tangential relative velocity, along with a return scheme for when the sticking assumption is violated. Plus, its time history must be stored during the whole duration of the contact. For a detailed algorithmic treatment, we refer to Campello [7].

The moments due to the friction forces (relatively to the center of the particle) are given by

$$\boldsymbol{m}_i^{fric} = \sum_{j=1}^{N_i^c} \boldsymbol{m}_{ij}^{fric}, \quad \text{with} \quad \boldsymbol{m}_{ij}^{fric} = \sum_{j=1}^{N_i^c} \boldsymbol{r}_{ij} \times \boldsymbol{f}_{ij}^{fric}, \tag{9}$$

where $\boldsymbol{m}_{ij}^{fric}$ is the moment on particle i due to its friction with particle (or object) j, and $\boldsymbol{r}_{ij} = r_i\boldsymbol{n}_{ij}$ is the vector that connects the center of particle i to its contact point with particle j.

The moments due to rolling resistance, in turn, are given by a spring-damper-slider model (often also called an "elastic-plastic" model), which may be thought of as the rotational version of the stick-slip friction model presented above. Accordingly, first we consider an elastic trial stick state in which the rolling resistance moment is

$$\boldsymbol{m}_i^{rol} = \sum_{j=1}^{N_i^c} \boldsymbol{m}_{ij}^{rol,\text{trial}}, \quad \text{with} \quad \boldsymbol{m}_{ij}^{rol,\text{trial}} = -8G^*\sqrt{r^*}\delta_{ij}^{1/2}(r^*)^2\Delta\boldsymbol{\theta}_{ij}^{\text{trial}} - d^{rol}\boldsymbol{\omega}_{ij}, \tag{10}$$

and then we verify it by a slip check against the static rolling (or "yield") limit:

$$\begin{cases} IF \;\; \left\|\boldsymbol{m}_{ij}^{rol,\text{trial}}\right\| \leq \mu_r r^* \left\|\boldsymbol{f}_{ij}^{con}\right\| \Rightarrow \boldsymbol{m}_{ij}^{rol} = \boldsymbol{m}_{ij}^{rol,\text{trial}} \;\; (\text{trial state is valid}); \\ IF \;\; \left\|\boldsymbol{m}_{ij}^{rol,\text{trial}}\right\| > \mu_r r^* \left\|\boldsymbol{f}_{ij}^{con}\right\| \Rightarrow \boldsymbol{m}_{ij}^{rol} = \mu_r r^* \left\|\boldsymbol{f}_{ij}^{con}\right\| \boldsymbol{r}_{ij} \;\; (\text{sliding occurs}). \end{cases} \tag{11}$$

In the above expressions, $\Delta\boldsymbol{\theta}_{ij}^{\text{trial}}$ is the pair´s trial rolling rotation, d^{rol} is a rolling damping constant (analogous to the contact and friction damping constants), and $\boldsymbol{\omega}_{ij} = \boldsymbol{\omega}_i - \boldsymbol{\omega}_j$ is the relative rolling velocity between the contacting pair. In (11), μ_r is the rolling resistance coefficient, whereas $\boldsymbol{r}_{ij} = \boldsymbol{\omega}_{ij}\left\|\boldsymbol{\omega}_{ij}\right\|^{-1}$ is the rolling sliding direction. Similarly as to the friction force, in the rolling resistance

moment the pair´s rolling rotation has to be computed through time integration of the pair´s relative rolling velocity, along with a return scheme for when the sticking assumption is violated. Plus, its time history must likewise be stored during the whole duration of the rolling contact. Again, for a detailed algorithmic treatment, we refer the reader to Campello [7].

Remark 1. The interaction between particles and rigid walls may be represented as a special case of that between particles, simply by taking the walls with infinite mass, radius, inertia and elastic parameters in the above force and moment expressions.

Remark 2. The particles´ elasticity modulus may vary with temperature, implying some sort of thermal softening (or stiffening). This is one source of coupling between the thermal and mechanical fields, and can be considered in a simple way as will be shown in subsection 3.5. Another source of coupling is the heat transfer between particles through conduction, which is dependent on the particles´ contact area and the distance between their centers – and thereby, on the particles´ positions and velocities, as was previously mentioned. This will be seen in subsection 3.2.

3 Consideration of thermal effects

With the intention to determine the thermal states of the particles, in the same lines of the discrete particle formulation for the mechanical fields, we assume that the temperatures are uniform within particles. This corresponds to a lumped thermal model and is valid as long as the particles are relatively small, such that their surface area is very large (in comparison to their interior volume) as to allow for a rapid exchange of heat with the surrounding medium – which is the case here. The energy balance for the i^{th} particle reads

$$\dot{K}_i + \dot{U}_i^{int} = P_i^{ext} + \dot{Q}_i^{ext} + \dot{Q}_i^{cond} + \dot{Q}_i^{conv} + \dot{Q}_i^{rad} \,, \tag{12}$$

where K_i is the particle´s kinetic energy, U_i^{int} is the particle´s internal (mechanical plus thermal) energy, P_i^{ext} is the mechanical power due to the external forces, Q_i^{ext} is the particle´s heat input from external devices (e.g., fire nozzles, burners, laser beams, electric currents, etc.), Q_i^{cond} is the particle´s heat flow due to conduction (upon contact with other particles and objects), Q_i^{conv} is the particle´s heat flow due to convection (by its surroundings) and Q_i^{rad} is the particle´s heat flow due to radiative effects. The kinetic energy is given by

$$K_i = \frac{1}{2} m_i \boldsymbol{v}_i \cdot \boldsymbol{v}_i \,, \tag{13}$$

with its time derivative being

$$\dot{K}_i = \underbrace{m_i \dot{\boldsymbol{v}}_i \cdot \boldsymbol{v}_i}_{mechanical\,power} . \tag{14}$$

Consistent with the DEM assumptions, the particle´s deformations (due to contacts with other particles and objects) are assumed to be very small, such that the mechanical part of the internal or stored energy is negligible. There remains only its thermal part, which means that

$$U_i^{int} = m_i C_i \theta_i \,, \tag{15}$$

where C_i is the specific heat of the particle and θ_i is the particle´s temperature. The time derivative of (15) yields

$$\dot{U}_i^{int} = m_i C_i \dot{\theta}_i \,. \tag{16}$$

The power due to the external forces is

$$P_i^{ext} = \boldsymbol{f}_i^{tot} \cdot \boldsymbol{v}_i \,, \tag{17}$$

where $\boldsymbol{f}_i^{tot}$ is the total force vector acting on the particle, which is the sum of all forces on the right-hand side of equation (1). From the balance of linear momentum on the particle, one has $m_i \dot{\boldsymbol{v}}_i = \boldsymbol{f}_i^{tot}$, and if this is inserted into equation (14) it follows that

$$\dot{K}_i = P_i^{ext} \,, \tag{18}$$

implying that these two terms cancel out each other in equation (12). As a consequence, and taking (16) into account, the energy balance of the particle reads

$$m_i C_i \dot{\theta}_i = \dot{Q}_i^{ext} + \dot{Q}_i^{cond} + \dot{Q}_i^{conv} + \dot{Q}_i^{rad} \,. \tag{19}$$

This expression is formally identical to equation (1), except that it is now a scalar equation. It is the governing equation for the system´s thermal field. Each one of its heat power (or heat flow per unit time) contributions is described in the subsections that follow.

3.1 Heat power due to external devices

The heat power provided by external devices (fire nozzles, burners, laser beams, electric currents, etc.) can be described through given (ad-hoc) expressions according to the type of device that is heating up the system. A general expression can rely in the form

$$\dot{Q}_i^{ext} = a_i I_i^{dev} \,, \tag{20}$$

where $0 \leq a_i \leq 1$ is the particle´s absorptance (or absorptivity, ratio of the absorbed to the incident heat power), which must be known, and I_i^{dev} is the device´s input power at the particle´s location, which must also be known. For, e.g., fire nozzles, one possible expression for I_i^{dev} is

$$I_i^{dev} = I_0 A_i \left(1 - \frac{z_i}{d_{\max}} \right), \tag{21}$$

where I_0 is the nozzle´s input intensity (power per unit area of the nozzle´s cross-section, which must be known), $A_i = \pi r_i^2$ is the particle´s "frontal" area (i.e., the area that is exposed to the nozzle´s power), $d_{\max}$ is the maximum penetration (or heating reach) of the nozzle within the bulk of the material (which must also be known) and $0 \leq z_i \leq d_{\max}$ is the particle´s depth with respect to the nozzle´s striking position (measured along the nozzle´s path-length, as indicated in Fig. 1). For laser beams, in turn, one possible expression for I_i^{dev} may be derived from the Lambert-Beer law, which states that the attenuation of incident light through a material (by both absorption and scattering) is exponentially dependent on the material´s thickness (or, more precisely, optical depth) and its attenuation coefficient. Accordingly, we write

$$I_i^{dev} = I_0 A_i e^{-\mu z_i} \,, \tag{22}$$

where I_0 is the laser´s input intensity (power per unit area of the beam´s cross section, which must be known), $A_i = \pi r_i^2$ is the particle´s frontal area, μ is the material´s attenuation coefficient (a bulk property determining how much the radiant power of the beam is reduced as it passes through the bulk of the material, with units of m^{-1}) and z_i is the particle´s depth w.r.t. the beam´s striking position (measured along the beam´s path-length, as indicated in Fig. 1).

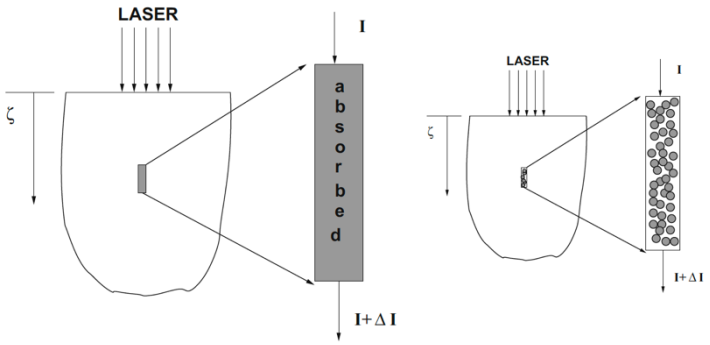

Figure 1. Representations of laser penetration based on modification (right) of the classical Beer–Lambert relation (left) **[18]**

We remark that considering the penetration of the heat source through the bulk of the material allows the deeper parts to be heated up more rapidly and effectively, and represents the physical process in a more reliable way. Other expressions for the device´s input power may be adopted, according to the problem at hand.

3.2 Heat power due to conduction

Heat flow through conduction in granular systems takes place whenever the particles contact other particles or objects (e.g., a wall with given temperature). It is a function of the temperature gradient between the contacting pair, the contact area between the pair and the pair´s individual thermal conductivities. Another important aspect lies in the determination of the contact area between particles (or particles and objects), which controls the amount of heat flow from one body to another. We follow the discrete form of Fourier´s law for conduction across interfaces, and adopt the following expression

$$\dot{Q}_i^{cond} = \sum_{j=1}^{N_i^c} \dot{Q}_{ij}^{cond}, \quad \text{with} \quad \dot{Q}_{ij}^{cond} = k_{ij} \frac{\theta_j - \theta_i}{\|\boldsymbol{x}_j - \boldsymbol{x}_i\|} A_{ij}^c, \tag{23}$$

where Q_{ij}^{cond} is the conduction heat flow on particle i due to its contact with particle (or object) j, N_i^c is the number of particles and objects that are in contact with particle i, k_{ij} is the effective thermal conductivity of the i-j contacting pair (which is a function of the individual thermal conductivities of i and j) and A_{ij}^c is the contact area between the pair. This latter is computed by assuming that the area is circular with radius a_{ij}, which in turn may be obtained through solution of the following geometrical problem (see Fig. 2):

$$\begin{aligned} a_{ij}^2 + L_i^2 &= r_i^2 \\ a_{ij}^2 + L_j^2 &= r_j^2 \\ L_i + L_j &= \|\boldsymbol{x}_j - \boldsymbol{x}_i\|, \end{aligned} \tag{24}$$

which gives (see Zohdi [14])

$$L_i = \frac{1}{2}\left(\|\boldsymbol{x}_j - \boldsymbol{x}_i\| - \frac{r_j^2 - r_i^2}{\|\boldsymbol{x}_j - \boldsymbol{x}_i\|}\right) \quad \Rightarrow \quad A_{ij}^c = \pi a_{ij}^2 = \pi(r_i^2 - L_i^2). \tag{25}$$

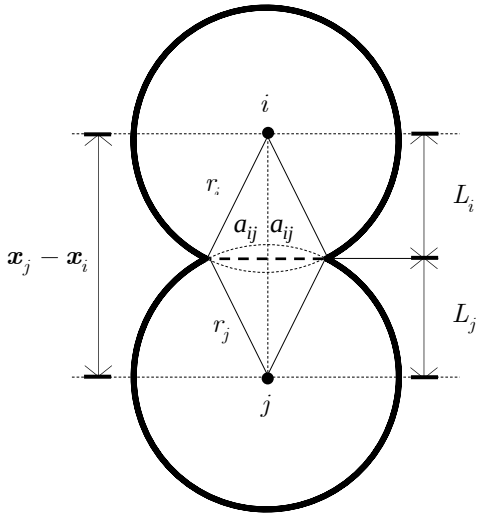

Figure 2. Geometrical representation of two contacting particles allowing for the solution to obtain L_i

The pair´s effective thermal conductivity may be computed from

$$\frac{r_i + r_j}{k_{ij}} = \frac{r_i}{k_i} + \frac{r_j}{k_j}\,, \tag{26}$$

where k_i and k_j are the thermal conductivities of i and j, respectively, and r_i and r_j their radii. Expression (26) is based on the assumption that the individual thermal resistances of the contacting particles may be summed up to provide the effective resistance of the pair, the reciprocal of which furnishes the pair´s effective conductivity. Note that (23) and (25) stand for a source of coupling between the thermal and mechanical fields, as it had been previously mentioned in a remark at the bottom of section 2.

3.3 Heat power due to convection

The surrounding environment (e.g., the environmental air) may exchange heat with the particles through convection (e.g., gas-particle). The corresponding amount can be computed through the classical Newton´s law of cooling. We adopt the following expression

$$\dot{Q}_i^{conv} = h_i(\theta_E - \theta_i)A_i^s\,, \tag{27}$$

where h_i is the convection (or film) coefficient of the particle w.r.t its surrounding environment, θ_E is the environment´s temperature at the particle´s location (which must be known) and $A_i^s = 4\pi r_i^2$ is total surface area of the particle. We assume that the convection coefficient is independent of the temperature difference between the particle and the environment. It may be computed by resorting to the Nusselt number Nu of the environment around the particle (ratio between its heat transfer of convection to heat transfer of conduction), such that

$$\mathrm{Nu} = \frac{h_i L}{k_E} \quad \Rightarrow \quad h_i = \frac{\mathrm{Nu}\, k_E}{L}, \tag{28}$$

where $L = 2r_i$ is the length scale and k_E is the environment´s thermal conductivity. The Nusselt number may be related to the Reynolds number and Prandtl number through the well-known heat transfer expression for flows past single spheres (see Whitaker [15])

$$\mathrm{Nu} \approx 2 + \ 0.4\,\mathrm{Re}^{1/2} + 0.06\,\mathrm{Re}^{2/3} \ \ \mathrm{Pr}^{0.4}\left(\frac{\mu_E}{\mu_{E,s}}\right)^{0.25}, \tag{29}$$

where

$$\mathrm{Pr} = \frac{C_E \mu_E}{k_E} \tag{30}$$

is the Prandtl number (wherein C_E is the environment´s specific heat), μ_E is the environment´s fluid viscosity and $\mu_{E,s}$ its viscosity at the particle´s surface temperature (we assume $\mu_{E,s} \approx \mu_E$ throughout this work). Expression (29) constitute a semi-empirical relation, and allows for a realistic estimate to the convection coefficient of smooth spheres for a wide range of heat transfer and fluid flow regimes. We remark that the above model is consistent with the small particles assumption.

3.4 Heat power due to radiation

For the particle sizes and types of materials we are interested in this work, the contribution of heat transfer by radiation may become relevant at moderate to high temperatures (over 1000 ºK) [5], considering that the particle´s surrounding environment (i.e., the environmental air) is at a significantly lower temperature. In such condition, the amount of electromagnetic thermal radiation that is emitted by a particle may be significantly larger than that absorbed by it from the environment, creating an outward net energy flow from the particles that ultimately promotes overall cooling of the system. We follow the Stefan-Boltzmann law to account for this effect, and adopt the following expression:

$$\dot{Q}_i^{rad} = \varepsilon_i B(\theta_E^4 - \theta_i^4) A_i^s \,, \tag{31}$$

where $0 \leq \varepsilon_i \leq 1$ is the particle´s radiative cooling efficiency (which must be known), $B = 5.670367 \times 10^{-8}$ W/m²·K⁴ is the Stefan-Boltzmann constant, θ_E is the environment´s temperature at the particle´s location (which must also be known) and $A_i^s = 4\pi r_i^2$ is the particle´s surface area. The environment´s temperature, besides being known (i.e., given), is assumed to be unaffected by the particle´s temperature. We once again remark that this is consistent with the small particles assumption.

3.5 Thermal softening of mechanical properties

Most materials have their mechanical properties degraded with increasing temperature. To incorporate such softening effects into the particles´ dynamics, one straightforward way is to consider temperature-dependent mechanical properties (e.g., by means of given input curves), instead of constant-valued ones. Accordingly, we adopt the following expression for the particles´ elasticity modulus:

$$E_i = \hat{E}_i(\theta_i) = \min\left\{E_0, E_0 e^{1-\frac{\theta_i}{\theta^*}}\right\}, \tag{32}$$

where E_0 is the modulus´ "ground" or reference value (e.g., the value at room temperature, or at a temperature interval around the room temperature) and θ^* is the critical temperature at which it starts to degrade. Fig. 3 depicts (qualitatively) the general behavior implied by this relation for a ground modulus of $E_0 = 1.0$ MPa and a critical temperature $\theta^* = 400$ K. One should notice that thermal softening affects not only the particle´s normal stiffness (and therefrom its normal contact forces), but also its tangential stiffness (and thus its friction forces and rolling resistance moments), since the elasticity modulus enters the expression of the particle´s shear modulus.

4 Numerical solution scheme

We adopt the explicit forward Euler scheme to compute the time evolution of the system. Integrating the governing equations (1) and (19) numerically between any two times instants t and $t+\Delta t$, for the velocities and spins of the particles we obtain

$$\begin{aligned}
\boldsymbol{v}_i(t+\Delta t) &= \boldsymbol{v}_i(t) + \frac{1}{m_i}\int_t^{t+\Delta t}(m_i\boldsymbol{g} + \boldsymbol{f}_i^{con} + \boldsymbol{f}_i^{fric})dt \\
&\approx \boldsymbol{v}_i(t) + \frac{\Delta t}{m_i}\ m_i\boldsymbol{g} + \boldsymbol{f}_i^{con}(t) + \boldsymbol{f}_i^{fric}(t)\ \ , \\
\boldsymbol{\omega}_i(t+\Delta t) &= \boldsymbol{\omega}_i(t) + \frac{1}{j_i}\int_t^{t+\Delta t}(\boldsymbol{m}_i^{fric} + \boldsymbol{m}_i^{rol})dt \\
&\approx \boldsymbol{\omega}_i(t) + \frac{\Delta t}{j_i}\ \boldsymbol{m}_i^{fric}(t) + \boldsymbol{m}_i^{rol}(t)\ \ ,
\end{aligned} \tag{33}$$

where Δt is the integration time step size, whereas for the positions and incremental rotations we have

$$\begin{aligned}
\boldsymbol{x}_i(t+\Delta t) &\approx \boldsymbol{x}_i(t) + \boldsymbol{v}_i(t+\Delta t)\Delta t\,, \\
\boldsymbol{\alpha}_i^{\Delta}(t+\Delta t) &\approx \boldsymbol{\omega}_i(t+\Delta t)\Delta t\,.
\end{aligned} \tag{34}$$

The total rotation vectors are obtained by means of the Rodrigues formula (see Campello [8])

$$\boldsymbol{\alpha}_i(t+\Delta t) = \frac{4}{4 - \boldsymbol{\alpha}_i(t)\cdot\boldsymbol{\alpha}_i^{\Delta}(t+\Delta t)}\left(\boldsymbol{\alpha}_i(t) + \boldsymbol{\alpha}_i^{\Delta}(t+\Delta t) - \frac{1}{2}\boldsymbol{\alpha}_i(t)\times\boldsymbol{\alpha}_i^{\Delta}(t+\Delta t)\right). \tag{35}$$

For the temperatures of the particles, in turn, we have

$$\begin{aligned}
\theta_i(t+\Delta t) &= \theta_i(t) + \frac{1}{m_i C_i}\int_t^{t+\Delta t}(\dot{Q}_i^{ext} + \dot{Q}_i^{cond} + \dot{Q}_i^{conv} + \dot{Q}_i^{rad} + \dot{Q}_i^{chem} + D_i^{imp})dt \\
&\approx \theta_i(t) + \frac{\Delta t}{m_i C_i}\ \dot{Q}_i^{ext}(t) + \dot{Q}_i^{cond}(t) + \dot{Q}_i^{conv}(t) + \dot{Q}_i^{rad}(t) + \dot{Q}_i^{chem}(t) + D_i^{imp}(t)\ \ .
\end{aligned} \tag{36}$$

The solution process is very straightforward, as schematically outlined in the algorithm below:

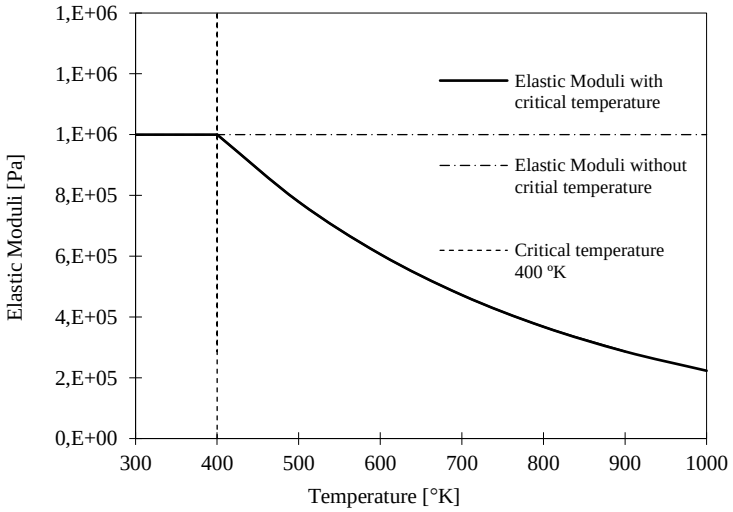

Figure 3. Schematic illustration of the thermal degradation of the particle's elasticity modulus as implied by the proposed relation.

1. Initialize time variables and get initial conditions:
   $t = 0$, $\Delta t =$ given
   $\boldsymbol{x}_i(0)$, $\boldsymbol{v}_i(0)$, $\boldsymbol{\omega}_i(0)$, $\boldsymbol{\alpha}_i(0)$, $\theta_i(0) =$ given.

2. Compute forces and moments at time t via equations (2), (7)-(8), (9) and (10)-(11), taking (32) into account.

3. Compute heat powers at time t via equations (20), (23), (27) and (31).

4. Freeze thermal field and update velocities, spins, positions and incremental rotations via equations (33) and (34).

5. Freeze mechanical fields and update temperatures through equation (36).

6. Save updated variables and move to next time step:
   $\boldsymbol{v}_i(t) \leftarrow \boldsymbol{v}_i(t + \Delta t)$,
   $\boldsymbol{\omega}_i(t) \leftarrow \boldsymbol{\omega}_i(t + \Delta t)$,
   $\boldsymbol{x}_i(t) \leftarrow \boldsymbol{x}_i(t + \Delta t)$,
   $\boldsymbol{\alpha}_i(t) \leftarrow \boldsymbol{\alpha}_i(t + \Delta t)$,
   $\theta_i(t) \leftarrow \theta_i(t + \Delta t)$,
   $t \leftarrow t + \Delta t$
   Go to step 2.

Remark 3. The use of implicit time integration schemes, such as the backward Euler scheme or the midpoint rule, is entirely possible within this framework (see, e.g., Zohdi [11] and Campello [8]). Here, however, since we are interested in having a "first working version" of the model in its simplest form, and since we are not concerned with long-term calculations (for which accuracy could be an issue), explicit, first-order accurate methods are sufficient. The implicit version is currently under development by the authors, using a recursive (fixed-point iterative) error-controlled approach within each time step, and will appear soon in a forthcoming paper.

5 Numerical examples

Now, we illustrate the usage of the above model by analyzing a few numerical examples. First, we show two simple validation problems involving only a small number of particles (we remark that extensive validation of the model has been conducted in a separate study, and will not be reported here). Then, we analyze a more general, multi-particle model-problem. We select the time step size in each example according to the following criterion, which is based on the expected duration of the particles´ contacts or collisions:

$$\Delta t \leq \frac{\delta t_{con}}{10}, \quad \delta t_{con} \cong 2.87 \left[\frac{(m^*)^2}{r^* (E^*)^2 v_{rel}} \right]^{1/5}, \tag{37}$$

where δt_{con} is the duration of a typical contact or collision and v_{rel} is the relative velocity of a typical contacting pair in the pair´s central direction immediately before the contact or collision is initiated. This is based on Hertz´s contact theory (see Johnson [13]) and, according to our experience, allows for a good accuracy in the integration of the contact forces. Contact detection is performed via a hybrid global-local search method, wherein both domain subdivision cells and nearest-neighbors lists ("Verlet lists") are combined.

5.1 Interaction between a particle and a thermal base

This example is analyzed to investigate the behavior of the basic ingredient of a thermomechanical particle system, namely, the interaction between two contacting objects. For simplicity, we consider here a single particle in contact with a thermal floor, with arbitrarily different initial temperatures. We want to assess some of the features of our scheme under simple idealized conditions, such that we may better highlight its coupled thermal-mechanical aspects. We want to assess the evolution of the particle´s temperature and the subsequent effect in its elastic stiffness and contact force. The particle has radius $r_1 = 0.001$ m and is placed tangentially over a thermally active base, as shown in Fig. 4. Gravity acts downwards.

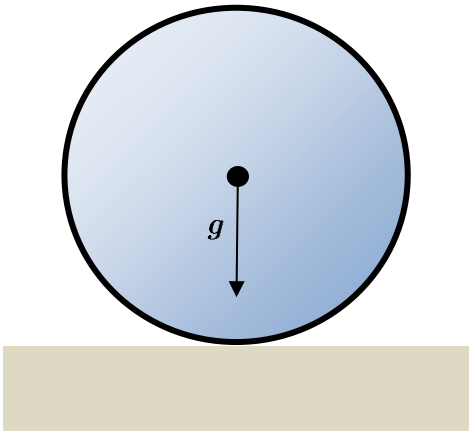

Figure 4. Single particle under gravity placed over a thermally active floor

The particle has an initial temperature $\theta_1(0) = 300\,^{\circ}\text{K}$ and is made of a material with thermal conductivity $k_1 = 60$ W/m·K, specific heat $C_1 = 100$ J/kg·K, mass density $\rho_1 = 3000$ kg/m^3 and elastic properties at room temperature $E_{0,1} = 1.0$ MPa and $\nu_1 = 0.3$, with a critical (degrading) temperature $\theta_1^* = 400\,^{\circ}\text{K}$. Critical damping is considered (i.e., $\xi^{con} = 1.0$). The floor is assumed to have infinite mass and zero conductivity (i.e. it does not change its temperature over time), with a (constant) temperature $\theta_f = 700\,^{\circ}\text{K}$. The surrounding environment is not considered (i.e,. it does not absorb nor provide heat to the particle). As gravity drives the particle towards the floor, they make contact and the particle starts to receive heat from the floor through conduction, due to their different temperatures. Eventually, the particle attains mechanical and thermal equilibrium with the floor. Figures 5-10 depict the evolution of the particle´s temperature with time, along with graphs of its overlap and contact area, elastic moduli and contact force with time. As we can see in Fig. 5, the thermal equilibrium is reached at around $t \approx 16$ s. The elastic moduli is clearly seen to degrade with time (Fig. 9), and the overlap consequently is seen to increase until thermal equilibrium with the floor is reached (Fig. 6). Another interesting aspect, as a consequence of the increase of the overlap, is the increment of the contact area (Fig. 7), of about 63%, if compared to the area when softening is not considered. This implies an increase on the amount of heat flow through conduction between both objects, as can be seen in Fig. 8. Therein, a reference line at $t = 8$ s is plotted in the graph, for which the temperature of the particle differs in about 7% when compared to the non-softening case. With regards to the contac force, the change in elastic modulus and overlap would make one to expect that the contact force also varies in time; however, it is seen from the graph in Fig. 10 that this does not happen: the force is perfectly constant in time, with a value of 1.23×10^{-4} N. It turns out that the decrease in stiffness is exactly compensated by the increase in the overlap, and the force remains constant thereby. Indeed, this is consistent with static equilibrium, since the only external force acting upon the particle is the gravity force, which is constant. The time step size adopted in this simulation was $\Delta t = 2 \times 10^{-5}$ s and the final time was $t = 40$ s.

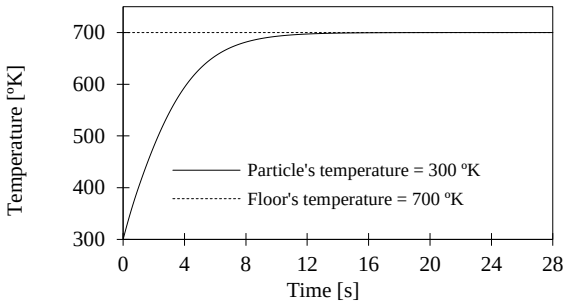

Figure 5. Evolution of the particle´s temperature

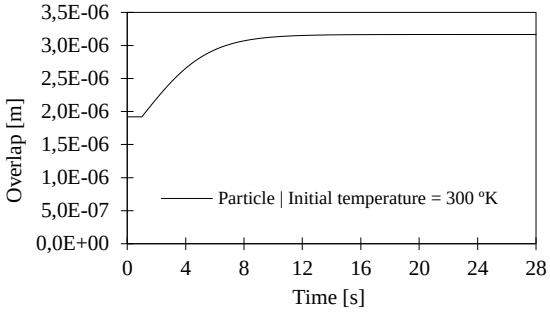

Figure 6. Evolution of the overlap with respect to time

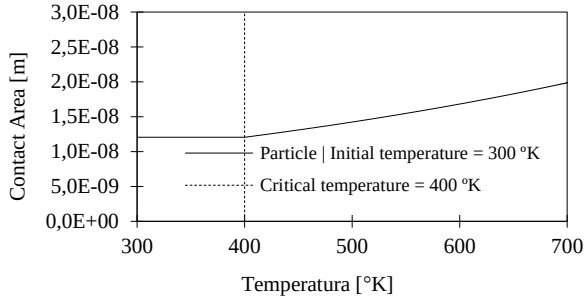

Figure 7. Increasing of the contact area of the particle as result of the thermal softening

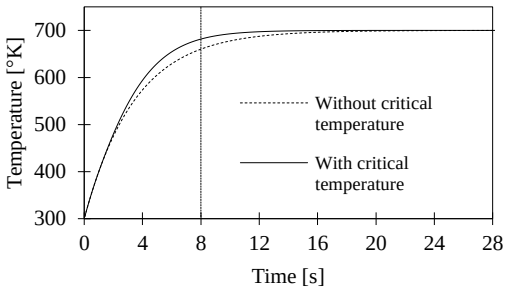

Figure 8. Evolution of the temperature considering the degradation of the elastic moduli

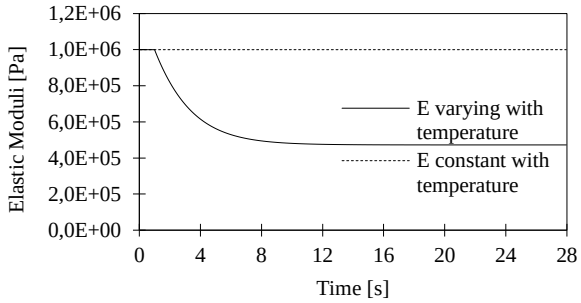

Figure 9. Evolution of the elastic moduli along time as the particle´s temperature varies

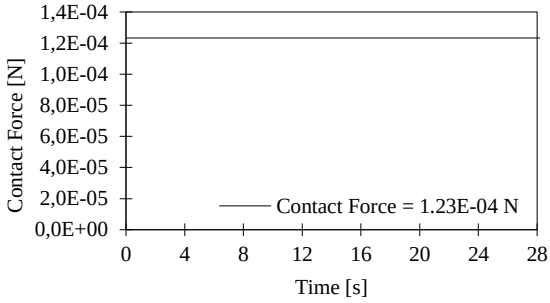

Figure 10. Evolution of the contact force

5.2 Conduction through a 2D particle assembly

In this case we want to reproduce an example proprosed by Feng et al. [16], with some slight modifications. The original example differs from ours in the sense that Feng et al.´s model is based on the thermal conductances of the contacting particles, instead of their thermal conductivities (this latter is a material property, whereas the former is a component-based one). Firstly, a 2D particle assembly is ramdomly generated within a recipient of length $L = 0.1$ m and height $H = 0.1$ m (recipient with lateral and bottom walls). The particles' radii are prescribed to follow a Gaussian distribution of mean $r_m = 0.003\,\mathrm{m}$ and standard deviation $\sigma_r = 0.000666\,\mathrm{m}$, with truncation limits set to $r_{\min} = r_m - 3\sigma_r = 0.001\,\mathrm{m}$ and $r_{\max} = r_m + 3\sigma_r = 0.005$ (this encompasses more than 99% of the distribution). Next, a temperature gradient is applied between the lateral (i.e., left and right) walls, to trigger heat flow between them. The walls are assumed to have inifinite thermal mass and zero conductivity, i.e., they only furnish heat to the particles (never change their temperature). Table 1 summarizies the initial conditions and the thermal properties of the problem. Gravity acts downwards.

Table 1. Initial conditions and thermal properties

Nº	Material	Initial temperature [ºK]	Thermal conductivity [W/m·K]	Specific heat [J/kg·K]	Mass [kg/m^3]
1	Particles	300	100	100	1000
2	Left wall	700	[*]	[*]	[*]
3	Right wall	300	[*]	[*]	[*]

[*] Walls´ thermal properties are irrelevant since they are prescribed to have constant temperature.

A sequence of snapshots at selected time instants are depicted in Fig. 11a-f in order to show the evolution of the temperatures across the particles as a consequence of the heat flow. In this case, the time step size adopted in the simulation was $\Delta t = 1 \times 10^{-4}$ s and the final time was $t = 300$ s.

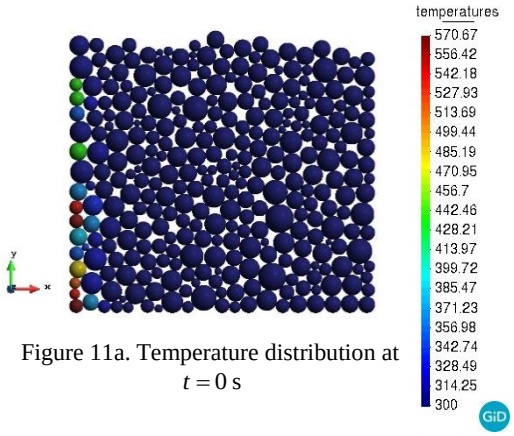

Figure 11a. Temperature distribution at $t = 0$ s

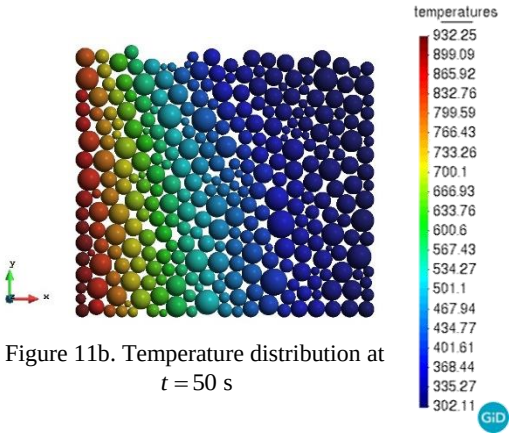

Figure 11b. Temperature distribution at $t = 50$ s

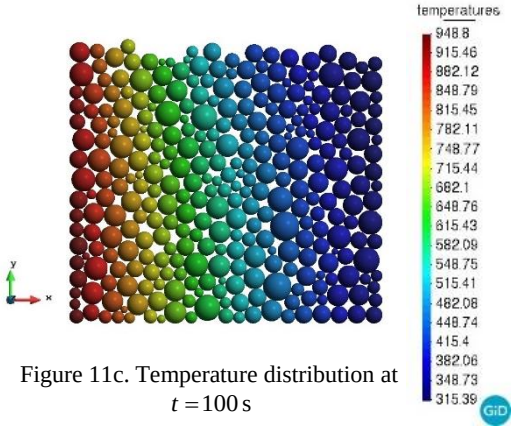

Figure 11c. Temperature distribution at $t = 100$ s

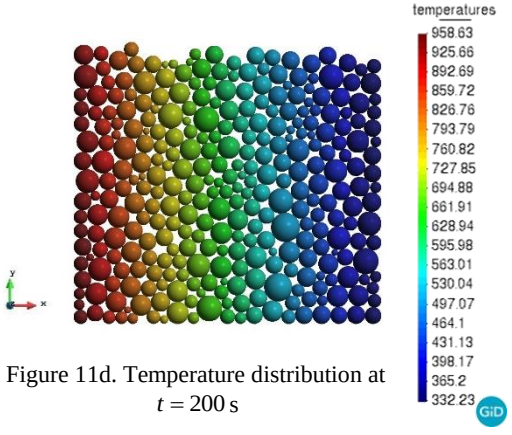

Figure 11d. Temperature distribution at $t = 200$ s

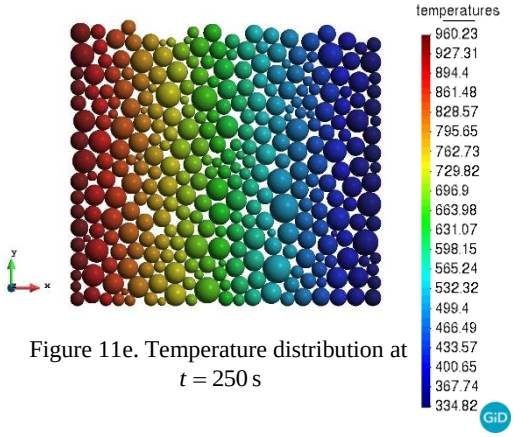

Figure 11e. Temperature distribution at $t = 250$ s

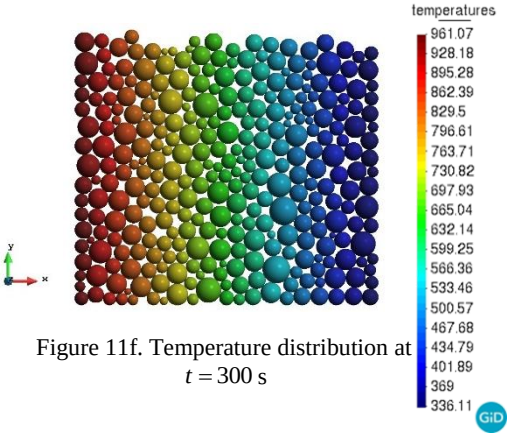

Figure 11f. Temperature distribution at $t = 300$ s

As we can see in Figs. 11a-f, there is a pronounced heat flow through the particles from left (where the wall has higher temperature) to right, as expected. Additionally, in the initial stages the heat flow is more pronounced where the contact between particles is denser (lower left side), as it can be seen from Figs. 11b-d. Another interesting aspect, as shown in Fig. 11f, is that once thermal equilibrium is reached, the heat flows more or less parallel to the lateral walls, which is also expected, given that the applied temperatures are constant along the lateral walls´ height and there is no heat applied to the bottom wall.

5.3 Laser-sintering of a bed of particles

This example has been proposed by Ganeriwala and Zohdi [17]. Here, we analyze it with some slight modifications: we consider Hertz-based contact, consistent stick-slip friction, consistent rolling resistance, as well as convection, radiation and termal softening of the elasticity modulus (instead of [17]´s no convection, no radiation and no thermal softening), but no phase transformation. To better highlight the effects of these phenomena, the particles´ diameters and bed´s lateral dimensions have been changed here in comparison to Ganeriwala and Zohdi´s original example. Accordingly, a bed of metalic particles whose properties are summarized in Table 2 is heated from above by a high-intensity laser beam. The laser moves in the horizontal z-direction at a constant speed of 1 m/s, as to heat the particles and promote their rapid sintering. Its properties are shown in Table 2. The beam´s intensity is assumed to be uniform throughout its cross-sectional area. Considering that the particles are very stiff, a small time step size of $\Delta t = 5 \times 10^{-7}$ s is adopted. The total simulation time is $t = 0.04$ s.

Table 2. Values used in the simulation

Nº	Parameter	Values
1	Particle´s diameter (mean, std. dev)	1.0 mm, 0.1 mm
2	Number of particles	6401
3	Particles´ initial temperatures	373 K
4	Particles´ degrading temperature	700 K
5	Particles´ material density	7800 kg/m^3
6	Particles´ elastic modulus and Poisson coeff.	200 GPa and 0.3
7	Particles´ friction and rolling resistance coeffs.	0.1
8	Particles´ damping rates	1.0
9	Bed´s lateral dimensions	40 mm x 40 mm
10	Laser power	5000 W
11	Laser beam diameter	10 mm
12	Laser beam horizontal velocity	1 m/s
13	Particles´ thermal conductivity	60 W/m.K
14	Particles´ heat capacity	600 J/kg.K

Figures 13a-f show a sequence of screenshots as obtained with our simulation. Results from Figs. 13a-d consider heat transfer only through conduction, whereas those from Fig. 13e, besides conduction, there is convection and radiation with the surroundings (in this case the environment is assumed to be at room temperature, i.e., 273 K). At $t = 0.04$ s, the average temperature of the particles targeted by the laser beam for the case with conduction only is 1127 K, whereas for the case with convection and radiation it is 1121 K (a difference of about 0.53%). As for the maximum particle temperatures, a difference of about 5% is seen between both cases. We remark that these differences shall increase for longer-time simulations (notice that the total simulation time is only $t_F = 0.04$ s here). Fig. 13f shows the laser beam returning after the first pass, following the reverse pattern of the previous figures (for brevity, this is shown only for the conduction-only case). Moreover, it can be seen in Fig. 12a that the average bed temperature increases lineraly as the laser passes over it. In the overall, one interesting aspect that can be seen in both cases is that the smaller particles heat up much quicker than the larger ones (see Figs. 12b,c), irrespective of their location at the bed´s height (they are not on the top layer and receive less energy for being smaller, but have much less thermal mass and thus heat up much faster once striken by the beam). Also, particles located near the boundaries of the beam´s cross-section heat up less than those inside the beam, due to conduction with the cooler neighboring particles.

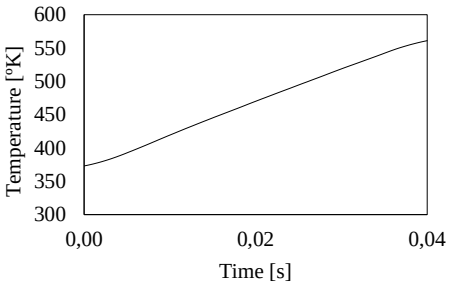

Figure 12a. Average of entire powder bed with time. Only conduction

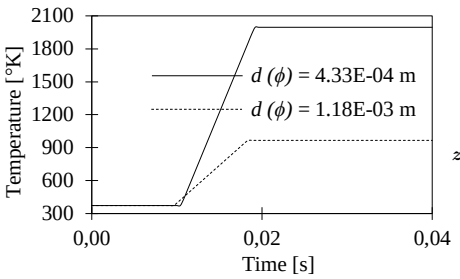

Figure 12b. Evolution of temperature of two neighbor particles with different diameters and same initial temperatures

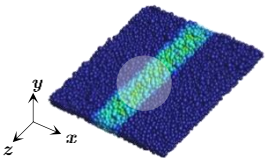

Figure 12c. Region where the neighbor particles are located

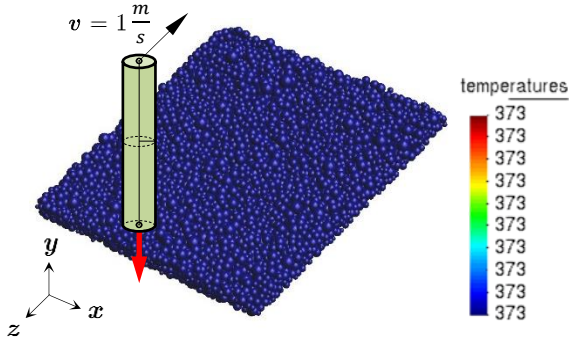

Figure 13a. Laser sintering at $t = 0$ s. Only conduction. Color represents temperatures in [ºK]

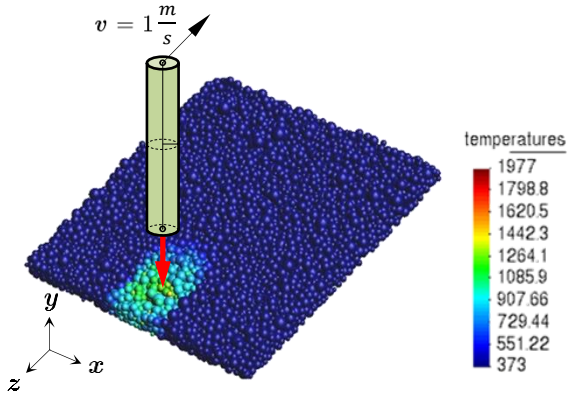

Figure 13b. Laser sintering at $t = 1 \times 10^{-2}$ s. Only conduction. Color represents temperatures in [ºK]

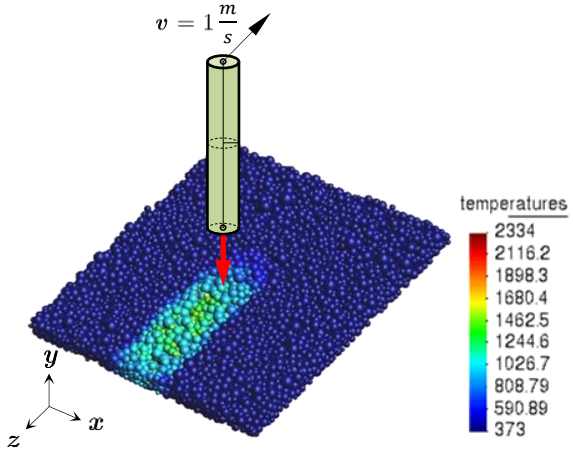

Figure 13c. Laser sintering at $t = 2 \times 10^{-2}$ s. Only conduction. Color represents temperatures in [ºK]

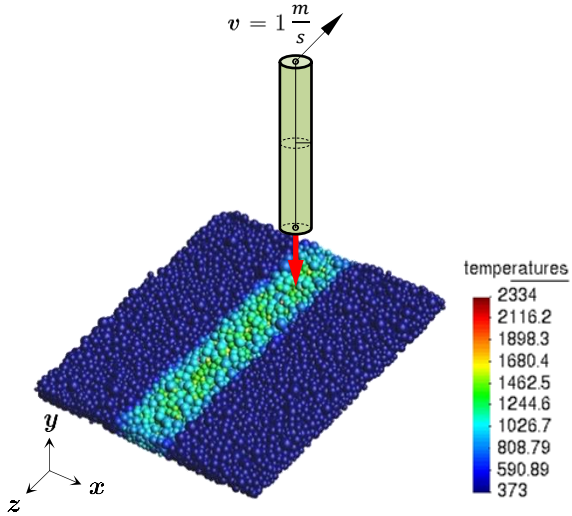

Figure 13d. Laser sintering at $t = 4 \times 10^{-2}$ s Only conduction. Color represents temperatures in [ºK]

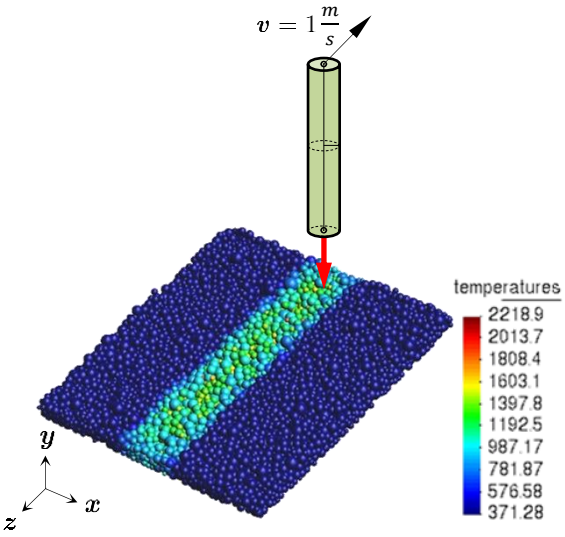

Figure 13e. Laser sintering at $t = 4 \times 10^{-2}$ s. Conduction, convection and radiation were considered. Color represents temperatures in [ºK]

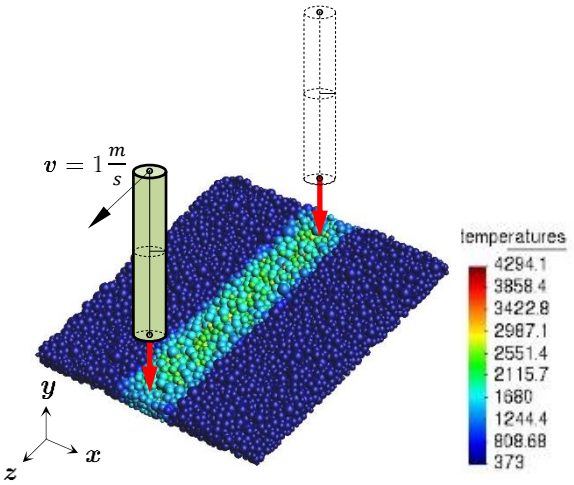

Figure 13f. Laser sintering at $t = 8 \times 10^{-2}$ s. Only conduction. Color represents temperatures in [ºK]

6 Conclusions

Modern industry, such as aerospace, military and state-of-the-art civil construction, have adopted advanced manufacturing (such as 3D printing and other particle deposition processes) as a rapid and efficient alternative for manufacturing industrial parts. These techniques invariably include thermally-active particles such as sintering powders and functionalized cementitious materials. From a mechanistic point of view, they form discrete particle systems, wherein the controlled heating (and further processing) of particles is critical. In order to have a reliable and fairly accurate representation of the behavior of such systems under external (thermal and mechanical) excitations, a multiphysical description is required. The purpose of this work was to present the first results of an on-going research, through which we are developing a multiphysics computational model for the simulation of such discrete particle systems. We find the model to be reasonably simple and straightforward to be implemented by engineers and analysts interested in the field. Also, as it could be seen from these first results, it proved to work very well for the purposes envisioned (we recall that extensive validation has been conducted in a separate study, and is not reported here). This truly motivates us to pursue in its advancement and extension. In this regard, incorporation other force contributions, such as adhesion and near-field (electromagnetic) interactions, as well as more complex heat phenomena such as phase transformation and chemical reactions, is currently under development by the authors. Likewise, the implicit version of the solution method is under construction. All these advancements over the present model shall appear soon in a forthcoming paper.

Acknowledgements. First author acknowledges scholarship funding from Itaipú Binacional, Brazil-Paraguay through BECAL (Programa Nacional de Becas de Postgrado en el Exterior "Don Carlos Antonio López"), under the grant 590/2016. Second author acknowledges support by CNPq (Conselho Nacional de Desenvolvimento Científico e Tecnológico), Brazil, under the grants 309748/2015-1 and 307368/2018-1.

References

[1] P. Richard, M. Nicodemi, R. Delannay, P. Ribière e D. Bideau, "Slow relaxation and compaction of granular systems," vol. 4, pp. 121-128, 2005.

[2] A. E. Moumen, M. Tarfaoui e K. Lafdi, "Additive manufacturing of polymer composites: Processing and modeling approaches," *Composites Part B : Engineering*, pp. 166-182, 2019.

[3] M. Cotteleer, J. Holdowsky e M. Mahto, "3D opportunity in aerospace and defense: Additive manufacturing takes flight | Deloitte Insights," Deloitte University Press, [Online]. Available: https://www2.deloitte.com/insights/us/en/focus/3d-opportunity/additive-manufacturing-3d-opportunity-in-aerospace.html. [Acesso em July 2019].

[4] F. Radjai e F. Dubois, Discrete-element modeling of granular materials, Wiley-ISTE, 2011, p. 496.

[5] W. L. Vargas-Escobar, *Discrete Modeling of Heat Conduction in Granular Media*, (Doctoral thesis). Pittsburgh: School of Engineering - University of Pittsburgh, 2002.

[6] H. P. Zhu, Z. Y. Zhou, R. Y. Yang and A. B. Yu, "Discrete particle simulation of particulate systems: a review of major applications and findings," *Chemical Engineering Science*, vol. 63, p. 5728–5770, 2008.

[7] E. M. B. Campello, "A computational model for the simulation of dry granular materials," *International Journal of Nonlinear Mechanics*, vol. 106, pp. 89-107, 2018.

[8] E. M. B. Campello, "A description of rotations for DEM models of particle systems," *Computational Particle Mechanics*, vol. 2, pp. 109-125, 2015.

[9] E. M. B. Campello, *Um modelo computacional para o estudo de materiais granulares*, (Habilitation thesis). São Paulo: Escola Politécnica da Universidade de São Paulo, 2016.

[10] T. Zohdi, Dynamics of charged particulate systems: modeling, theory and computation, New York: Springer, 2012.

[11] T. Zohdi, "Additive particle deposition and selective laser processing - A computational manufacturing framework," *Computational Mechanics*, vol. 54, pp. 171-191, 2014.

[12] J. Duran, Sands, Powders and Grains: An introduction to the physics of granular matter, New York: Springer, 1997.

[13] K. L. Johnson, Contact Mechanics, Cambridge: Cambridge University Press, 1985.

[14] T. Zohdi, "A direct particle-based computational framework for electrically-enhanced thermo-mechanical sintering of powdered materials," *Mathematics and Mechanics of Solids*, vol. 19, no. 1, pp. 93-113, 2014.

[15] S. Whitaker, "Forced convection heat transfer correlations for flow in pipes, past flat plates, single cylinders, single spheres, and flow in packed beds and tube bundles," *AIChE Journal*, vol. 18, p. 361371, 1972.

[16] Y. T. Feng, K. Han and D. R. J. Owen, "Discrete thermal element modeling of heat conduction in particle systems: Pipe-network model and trasient analysis," *Powder Technology*, vol. 193, pp. 248-256, 2009.

[17] R. Ganeriwala and T. I. Zohdi, "Multiphysics modeling and simulation of selective laser sintering manufacturing processes," in *Procedia CIRP 14 (6th CIRP International Conference on High Performance Cutting, HPC2014)*, Berkeley, USA, 2014.

[18] T. I. Zohdi, Modeling and simulation of functionalized materials for additive manufacturing and 3D printing: continuous and discrete media, New York: Springer International Publishing, 2018.

[19] E. M. B. Campello, "Effect of particle spin on the spatio-thermal distribution of incandescent materials released from explosions," *Journal of the Brazilian Society of Mechanical Sciences and Engineering*, vol. n/a, p. n/a, 2019 (to appear).